Arch. Min. Sci. **63** (2018), 2, 491-509

Electronic version (in color) of this paper is available: http://mining.archives.pl

DOI 10.24425/122909

NEBOJŠA GNJATOVIĆ*#, SRĐAN BOŠNJAK*, ALEKSANDAR STEFANOVIĆ*

THE DEPENDENCY OF THE DYNAMIC RESPONSE OF A TWO MAST BUCKET WHEEL EXCAVATOR SUPERSTRUCTURE ON THE COUNTERWEIGHT MASS AND THE DEGREE OF FOURIER APPROXIMATION OF THE DIGGING RESISTANCE

ZALEŻNOŚĆ ODPOWIEDZI DYNAMICZNEJ KONSTRUKCJI DWUMASZTOWEJ KOPARKI KOŁOWEJ OD MASY PRZECIWCIĘŻARU ORAZ STOPNIA APROKSYMACJI OPORU URABIANIA ZA POMOCĄ SZEREGU FOURIERA

Sensitivity analysis of the dynamic response of both the designed and the actual models of a slewing superstructure with two masts to the variation of the counterweight mass and the degree of accuracy of the approximation polynomials of the digging resistance was conducted in the paper. Spatial reduced dynamic models of the bucket wheel excavator SchRs 1600 were used as a basis for the presented investigations. Based on the comparative analysis of the calculation results, the following conclusions were drawn: (a) mass of the counterweight has a significantly higher influence on the maximum intensities of accelerations of the referent points than on the spectrum of natural frequencies, (b) the accuracy of approximations of the digging resistance and the maximum values of accelerations differ by an order of magnitude, for the approximation trigonometric polynomial of the same number of harmonics.

Keywords: bucket wheel excavator, dynamic response, counterweight mass variation, digging resistance approximation

W pracy przeprowadzono analizę wrażliwości odpowiedzi dynamicznej modelu obliczeniowego i rzeczywistego konstrukcji obrotowej koparki z dwoma masztami na zmiany masy przeciwciężaru oraz zmiany stopnia dokładności przybliżania wielomianów określających opory urabiania. W pracy wykorzystano przestrzenne zredukowane modele dynamiczne koparki kołowej SchRs1600. Na podstawie analizy porównawczej wyników obliczeń wyciągnięto następujące wnioski: (a) masa przeciwciężaru ma znacznie większy wpływ na maksymalne natężenie przyspieszeń w punktach odniesienia niż na zakres częstotliwości własnych; (b) dokładność przybliżenia oporów urabiania i maksymalne wielkości przyspieszeń różnią się o rząd wielkości dla procedury aproksymacji wykorzystującej wielomian zawierający funkcje trygonometryczne, o tej samej liczbie harmonicznych.

Słowa kluczowe: koparka kołowa, odpowiedź dynamiczna, zmiany masy przeciwciężaru, przybliżone obliczenia oporu urabiania

* UNIVERSITY OF BELGRADE, FACULTY OF MECHANICAL ENGINEERING, KRALJICE MARIJE 16, 11120 BELGRADE, SERBIA

\# Corresponding author: ngnjatovic@mas.bg.ac.rs

Nomenclature

BWE	Bucket wheel excavator
BW	Bucket wheel
BWC	Bucket wheel centre
CW	Counterweight
COG	Centre of gravity
DOF	Degree of freedom
$i = 1,2,...,64$	Number of DOFs
q_i	Generalized coordinate
$q_{BW,V}$ and $q_{BW,L}$	Vertical and lateral displacements of the BWC
$a_{BW,V}$ and $a_{BW,L}$	Vertical and lateral accelerations of the BWC
$q_{CW,V}$ and $q_{CW,L}$	Vertical and lateral displacements of the CW COG
$a_{CW,V}$ and $a_{CW,L}$	Vertical and lateral accelerations of the CW COG
n=1,2,...,5	Number of harmonics of the trigonometric polynomials used to approximate the digging resistance
$f_{n,e}$	Frequency of excitation
M_T	Moment of excavation
M_{TN}	Nominal moment of excavation
M_{TF}	Approximated nominal moment of excavation via Fourier series
$m_{CW,DES}$	Mass of the CW according to the BWE project documentation
$m_{CW,ACT}$	Mass of the CW derived from the weighing results
Δm_{CW}	Lumped mass inserted into the CW COG
b	Dimensionless coefficient calculated as the ratio of Δm_{CW} and $m_{CW,ACT}$
b_{DES}	Value of the coefficient b for which $\Delta m_{CW} = m_{CW,DES}$
b_{ACT}	Value of the coefficient b for which $\Delta m_{CW} = m_{CW,ACT}$
Δm_S^{V3}	Excessive mass defined in (Bošnjak et al., 2016)
M1	Dynamic model without the excessive mass
M2	Dynamic model with the excessive mass
$n = 1,2,...,13$	Number of analyzed natural frequencies of the models
f_n	Natural frequency
$f_n^{b_{DES}}$	Value of the natural frequency obtained for $b = b_{DES}$
$f_n^{b_{ACT}}$	Value of the natural frequency obtained for $b = b_{ACT}$
DI	Designed image of the superstructure – model M1 with CW mass equal to $m_{CW,DES}$
AI	Actual image of the superstructure – model M2 with CW mass equal to $m_{CW,ACT}$
f_n^{DI}	Natural frequency obtained for DI
f_n^{AI}	Natural frequency obtained for AI
ψ	Ratio between the value of excitation frequency and the value of natural frequency
$a_{V,per}$	Permitted value of vertical acceleration according to the standard (DIN 22261-2, 2016)

$a_{L,per}$	Permitted value of lateral acceleration according to the standard (DIN 22261-2, 2016)
$a_{m,CW,ACT}$	Maximum generalized acceleration obtained for $\Delta m_{CW} = m_{CW,ACT}$
$a_{m,CW,DES}$	Maximum generalized acceleration obtained for $\Delta m_{CW} = m_{CW,DES}$
$a_{n=2}$	Maximum generalized acceleration obtained when the digging resistance approximation polynomial contains two excitation harmonics
$a_{n=5}$	Maximum generalized acceleration obtained when the digging resistance approximation polynomial contains five excitation harmonics
$a_{max,DI,n}$	Maximum generalized acceleration of the DI obtained when the digging resistance approximation polynomial contains n excitation harmonics
$a_{max,AI,n}$	Maximum generalized acceleration of the AI obtained when the digging resistance approximation polynomial contains n excitation harmonics

1. Introduction

Bucket wheel excavators (BWEs), machines operating in harsh working conditions, under the influence of loads of pronounced dynamic and stochastic nature, have a key role in surface mining systems. Tendencies towards increasing their capacities (Bošnjak, 2015; Che & Chen, 2014) and enabling excavation of soil of higher workability classes (Machniak & Kozioł, 2017) have not been adequately supported by the calculation methods. Inevitable reconstructions, conducted as a consequence of various types of technological (Bošnjak & Zrnić, 2012) and structural (Bošnjak & Zrnić, 2012; Rusiński et al., 2010) failures, as well as failures of vital mechanisms (Dudek et al., 2011; Savković et al., 2011) represent a solid proof of this statement.

Determination of the character and intensity of the external load caused by the resistance to excavation is, on its own, a very complex problem. Solving it requires a solution to three subproblems, related to (Bošnjak et al., 2006): (1) dimensions of the chip cross section; (2) specific resistance to excavation; (3) disposition of components of the resistance to excavation. The problems of determining the dimensions of the chip cross section and the disposition of components of the resistance to excavation, for the most general configuration of the working device, are successfully solved by applying the model presented in (Bošnjak, 2015). Having in mind the fact that the specific resistance to excavation represents a fundamental source of stochasticity in the BWE system, its temporary values are simulated with a random number generator (Bošnjak et al., 2006). In the citied paper, results of calculation of the influence of the digging resistance (treated both deterministically and stochastically) are presented and compared with the results of the corresponding measurements conducted ‘in situ’. Actual dimensions of the chip cross section differ from those determined using the kinematic model of the BWE working device. This is the consequence of vibrations of the bearing structure and the superstructure slewing mechanism. The model presented in (Bošnjak, 2015) enables coupling of the excitation and the system response, which leads to a principle change in the character of the BWE mathematical model. Namely, some of the stiffness coefficients become stochastic time dependant variables, i.e. the mathematical model of the BWE becomes rheolinear (Bošnjak et al., 2006). In the said paper, the evaluation of the rheolinear level and the level of stochasticity of the dynamic parameters of the model of the BWE SchRs 1760 was conducted.

Dynamic response represents a fundamental indicator of the behaviour of BWEs during exploitation (Cireş & Nani, 2016; Pietrusiak, 2017; Rusiński et al., 2017; Schlecht, 2014). Although they do not prescribe the procedures for their identification, the standards (AS4324.1, 1995; DIN 22261-2, 2016) do define the maximum values of accelerations of referent points of the superstructure, which implicates a necessity for the dynamic behaviour analysis in both the design phase and during reconstructions, which are relatively frequent during perennial exploitation (Bošković et al., 2015; Brkić et al., 2014; Gottvald, 2010; Rusiński et al., 2012). These were the primary motives to present the results of a sensitivity analysis of the BWE SchRs 1600, Fig. 1, superstructure response to the variation of the counterweight (CW) mass and the degree of accuracy of the trigonometric approximation polynomials of the digging resistance in the paper.

Fig. 1. BWE SchRs 1600: total mass (with mobile conveyor) 3345 t, mass of the superstructure 1233 t, theoretical capacity 6600 m^3/h

2. Dynamic model

The analysis of the dynamic behaviour of the BWE SchRs 1600 superstructure was performed on the basis of a reduced spatial dynamic model with 64 DOF. The model was developed and validated according to the procedures presented in (Bošnjak et al., 2006; Bošnjak & Gnjatović, 2016; Gnjatović, 2016). Validation of the said procedure, which supplements the finite element method in its application in the dynamic behaviour analysis of the BWE spatial truss structures, has been performed on the basis of relevant measurements. A concise overview of the stages in the process of validation of both the modelling procedure and the superstructure model of the BWE SchRs 1760 has been presented in (Bošnjak & Zrnić, 2012). A model formed in such a manner was subjected to the analysis of the dynamic behaviour in the out-of-resonance region (Bošnjak et al., 2015). It is therefore concluded that the process of modelling of the BWE superstructure, which has been rigorously applied for the development of the spatial reduced dynamic model of the SchRs 1600 superstructure, used as the basis for the research presented in this paper, has received both scientific and professional validation. The model, presented in Fig. 2, enables modal analysis as well as analysis of the dynamic response in a continuous domain of both constructional and parameters of excitation variation. Although BWEs are constructions

with changeable configuration, which makes the analysis of their dynamic behaviour extremely complex (Bošnjak & Gnjatović, 2016; Gottvald, 2011), according to the findings presented in (Gnjatović, 2016), the influence of the BW boom inclination angle on modal characteristics of the analyzed excavator is not significant. Thus, the horizontal position of the BW boom has been adopted as referent for further analysis.

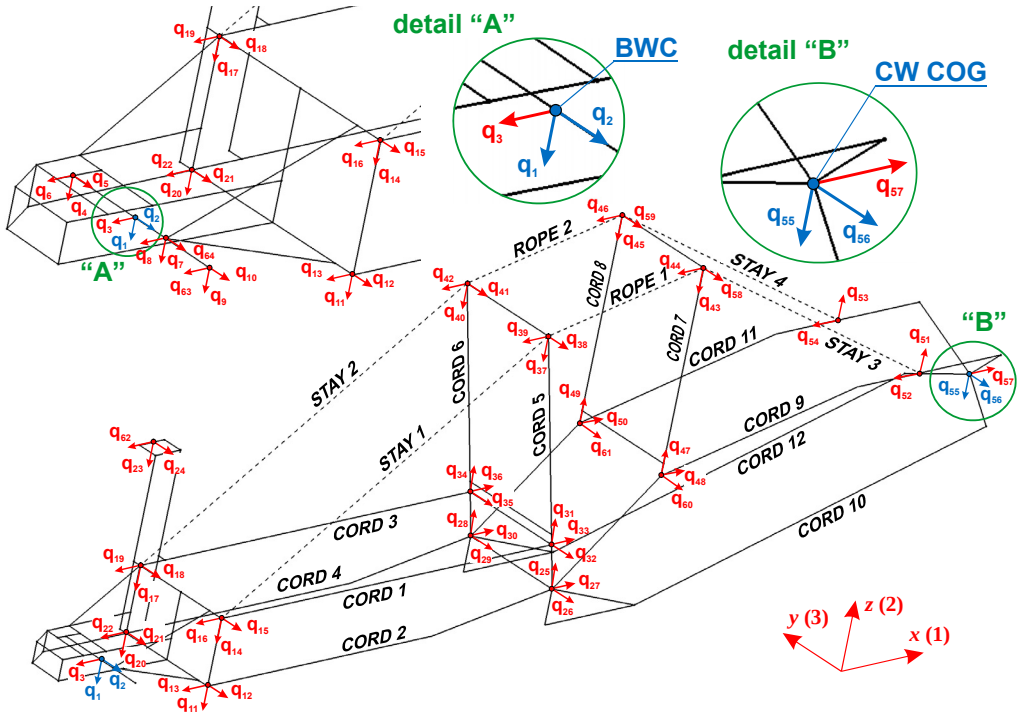

Fig. 2. Reduced spatial dynamic model of the BWE SchRs 1600 slewing superstructure: $q_{BW,V} = q_1$, $q_{BW,L} = q_2$ – vertical and lateral displacement of the BW centre; $q_{CW,V} = q_{55}$, $q_{CW,L} = q_{56}$ – vertical and lateral displacement of the CW COG

Having in mind the following facts:

(a) the influences of the CW mass and the degree of Fourier approximation of the digging resistance on the dynamic response of the BWE SchRs 1600 superstructure are investigated in the paper;

(b) during the exploitation of the BWE SchRS 1600, the appearance of parametric oscillations has not been observed;

identification of the external loads caused by the resistance to excavation was performed according to the procedures presented in (Rasper, 1973; Volkov & Cherkasov, 1969). The obtained external loads were approximated with trigonometric polynomials with $n = 1,2,...,5$ harmonics, using the Fourier coefficients. The ratios between the maximum values of mentioned trigonometric polynomials and the nominal maximum moment of excavation ($M_{TN,max} = 3093$ kNm) are presented in Fig. 3 and Table 1.

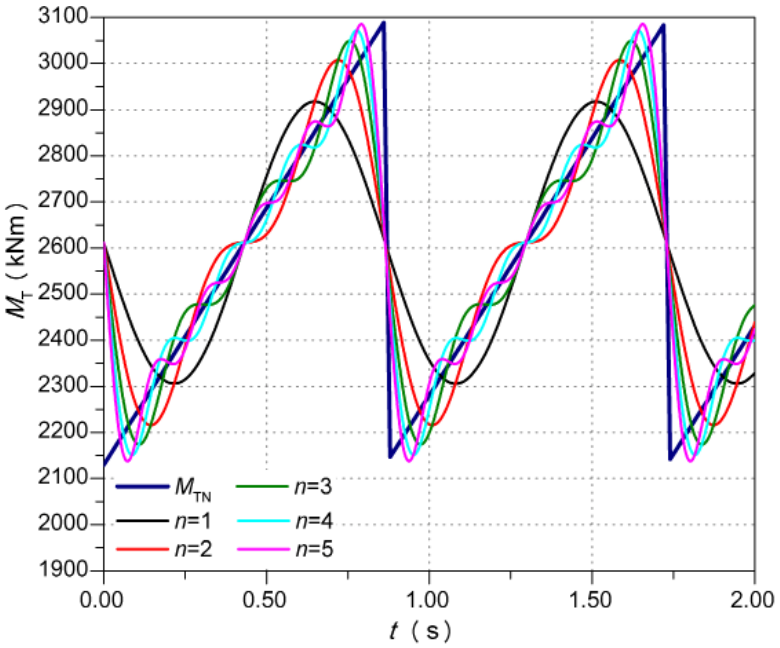

Fig. 3. Moment of excavation (M_T)

TABLE 1

Dependence of maximum moment of excavation values on the number of harmonics used for the approximation

Number of harmonics (n)	**$M_{TF,max}$ (kNm)**	$\frac{M_{TF,max} - M_{TN,max}}{M_{TN,max}} \times 100(\%)$
1	2918	–5.66
2	3010	–2.68
3	3054	–1.26
4	3080	–0.42
5	3097	+0.13

Finally, due to the extreme complexity of the dynamic system and the fact that, in practice, free vibration responses are quickly attenuated (Bošnjak et al., 2015), the forced response of the model was determined by applying the Lagrange's second order equations, under the assumption that the structural damping may be considered negligible in the out-of-resonance region.

Under the previously defined assumptions, the system of differential equations of motion yields to

$$\mathbf{M}(b)\cdot\ddot{\mathbf{q}}(b,n,t)+\mathbf{K}\cdot\mathbf{q}(b,n,t)=\mathbf{Q}_{\Omega}(n,t)$$

where:

M(b) — mass matrix whose coefficients were derived from the expressions for calculation of the kinetic energy of all superstructure subsystems established in (Gnjatović,

2016). It is important to note that chords of the BW and CW booms, and also of both masts, as dominant structural elements of the superstructure spatial truss structures, were treated as girders with continuous mass distribution, and their dynamic deflection lines were approximated by applying a local linearization (the method presented in (Bošnjak et al., 2006; Bošnjak & Gnjatović, 2016)). When the influence of the CW mass is analyzed over a continuous domain, the mass matrix becomes a matrix of functions dependent on the parameter b, defined in Section 3 of this paper;

$\mathbf{K}$ — stiffness matrix, obtained from the flexibility matrix whose coefficients were defined based on the response of the finite element model, presented in (Gnjatović, 2016), to a unit force applied on the referent nodes in the directions of the generalized coordinates;

$\{\mathbf{Q}_{\mathbf{\Omega}}(n,t)\}$ — vector of generalized non-potential forces of the system, derived from the expression for virtual work of the non-potential active loads presented in (Gnjatović, 2016);

$n = 1,2,...,5$ — number of harmonics of the trigonometric polynomials used to approximate the digging resistance;

$\ddot{\mathbf{q}}(b,n,t)$ and $\mathbf{q}(b,n,t)$ — vectors of generalized accelerations and displacements.

Indirect validation of the used reduced spatial dynamic model, Fig. 2, i.e. validation of the natural frequencies' values obtained by calculation and the respective modal deflection shapes, Fig. 4, was conducted by comparison with the results published in (Gottvald, 2010; 2011; Pietrusiak, 2013; Pietrusiak et al., 2014). Results of the numerical-experimental research on the dynamic characteristics of BWEs of the same design conception (BWEs with two masts) have been presented in the cited literature.

First vibration mode, Fig. 4(a), which represents vertical oscillations of the entire dynamic system, is in full compliance with the experimentally and numerically obtained modal deflection shapes of the BWE SchRs 1320 (Figs. 12 and 13 in (Gottvald, 2010)) and the BWE SchRs 4600.50 (Fig. 51.2(a) in (Pietrusiak et al., 2014)). Horizontal oscillations of the system are dominant in the second and third natural modes for all of the considered BWEs, Figs. 4(b) and 4(c) (see Figs. 12 and 13 in (Gottvald, 2010) and Figs. 51.2(b), 51.2(c) and 51.5 in (Pietrusiak et al., 2014)). Combination of vertical oscillations of the system and torsional oscillations of the BW boom, manifested in the fourth vibration mode, Fig. 4(d), is also experimentally obtained for the BWE SchRs 4600.50 (Fig. 51.11 in (Pietrusiak et al., 2014)). Values of natural frequencies obtained by calculation for the analyzed BWE are of the same order of magnitude as those used for comparison, but higher, which is explained by the fact that the masses of the latter (Gottvald, 2011; Pietrusiak, 2013) are greater than that of the analyzed BWE, Fig. 1.

The analysis to follow was conducted on the basis of the dynamic response of two referent points: (a) bucket wheel centre (BWC – a point of intersection of the BW vertical plane of symmetry across the buckets and the axis of the bucket wheel shaft) and (b) counterweight centre of gravity (CW COG), Fig. 2. This kind of approach is justified since previous investigations (Bošnjak & Zrnić, 2012; Bošnjak et al., 2015; Gnjatović, 2016; Gottvald, 2012; Pietrusiak, 2013; Rusiński et al., 2015) have shown that these referent points are most sensitive to the variation of excitation parameters and the mass of the CW.

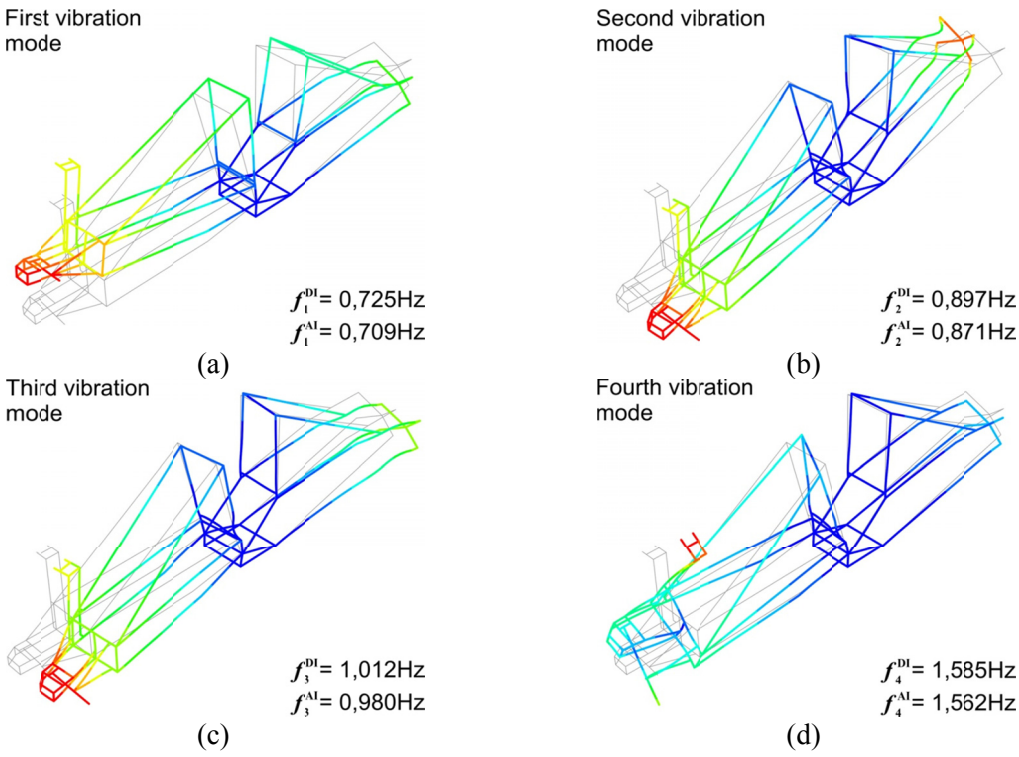

Fig. 4. Modal deflection shapes of the BWE SchRs 1600 reduced spatial dynamic model

3. Dynamic behaviour of the ‘a priori’ and ‘a posteriori’ models in case of continuous variation of the CW mass

For the purpose of the presented analyses, the influence of the CW mass was accounted for by inserting a lumped mass $\Delta m_{CW} = b m_{CW,ACT}$, $0.8 \leq b \leq 1.2$, into the CW COG. Although the designed ($m_{CW,DES}$ = 197 t) and actual ($m_{CW,ACT}$ = 238 t) masses of the CW are achieved for values of parameter b_{DES} = 0.83 and b_{ACT} = 1 respectively, the parameter was varied in a wider range in order to assess the influence of any additional increase of the CW mass on the dynamic behaviour of the system. The investigations were conducted for both ‘a priori’ and ‘a posteriori’ models, Figs. 5-8, Tables 2-5.

The spectrum of natural frequencies of the model was adopted in a way that accounts for the first five frequencies of excitation, i.e. those excitation harmonics with a sufficient energy potential to excite a resonant state of the vital structural elements.

Transformation from the ‘a priori’ (M1) to the ‘a posteriori’ (M2) model was realized by including the excessive mass of Δm_S^{V3} = 16.980 t as a lumped mass with coordinates defined in (Bošnjak et al., 2016).

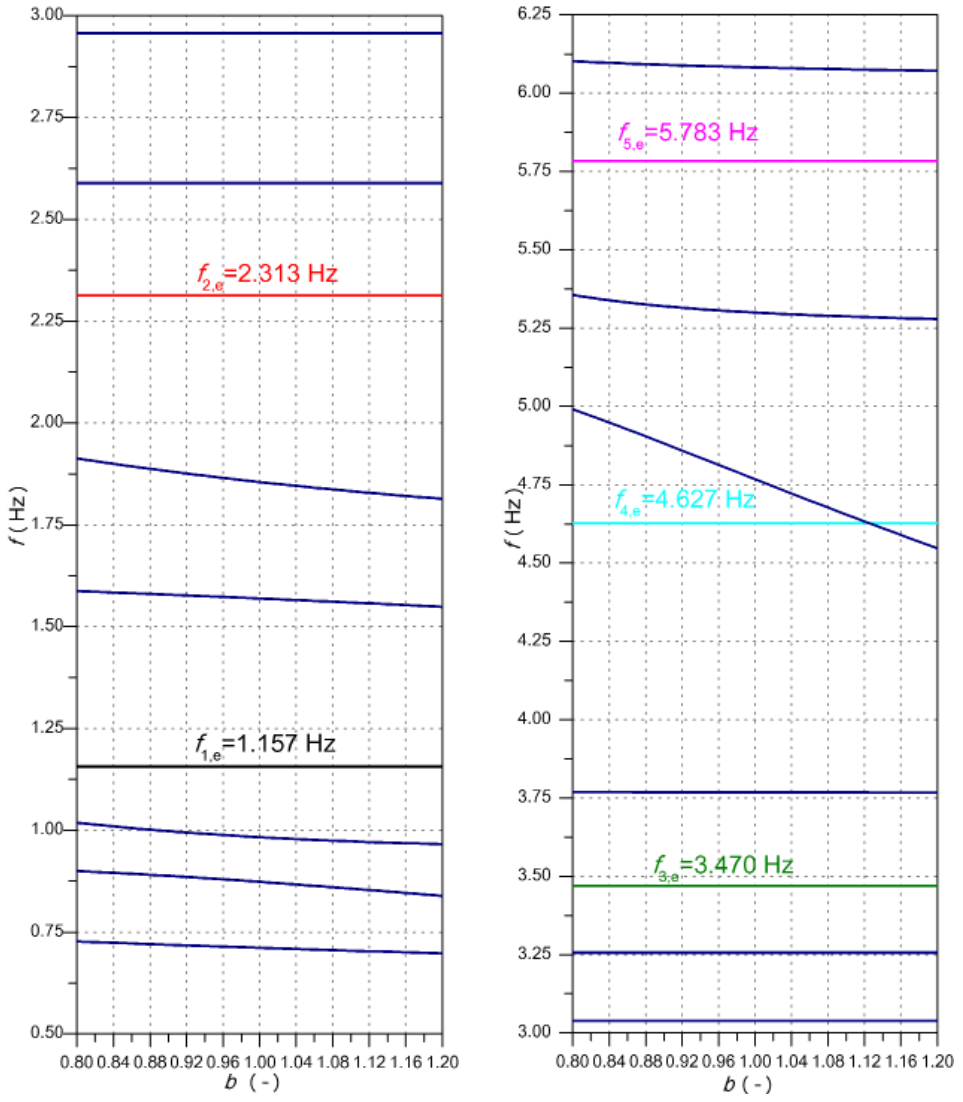

Fig. 5. Dependence of natural frequencies on the CW mass – model M1 (free vibration frequencies are in dark blue; for forced vibration frequencies see Fig. 3): (a) frequency spectrum 0.5 to 3 Hz, (b) frequency spectrum 3 to 6.25 Hz

TABLE 2

Influence of the CW mass on the spectrum of natural frequencies – model M1

f_n (Hz)	f_1	f_2	f_3	f_4	f_5	f_6	f_7	f_8	f_9	f_{10}	f_{11}	f_{12}	f_{13}
$m_{CW,DES}$	0.725	0.897	1.012	1.585	1.904	2.589	2.957	3.039	3.257	3.768	4.961	5.344	6.098
$m_{CW,ACT}$	0.712	0.873	0.983	1.569	1.855	2.589	2.957	3.039	3.257	3.768	4.768	5.3	6.082

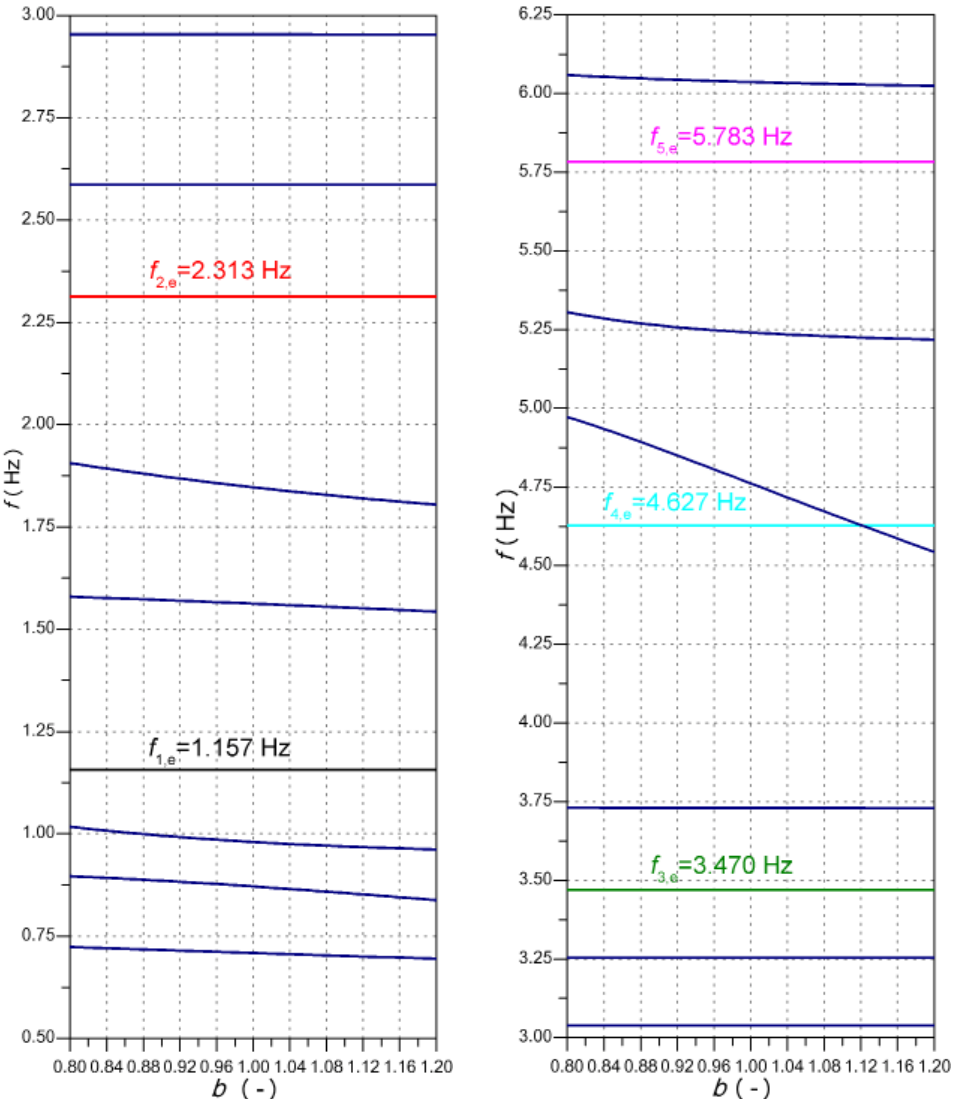

Fig. 6. Dependence of natural frequencies on the CW mass – model M2 (free vibration frequencies are in dark blue; for forced vibration frequencies see Fig. 3): (a) frequency spectrum 0.5 to 3 Hz, (b) frequency spectrum 3 to 6.25 Hz

TABLE 3

Influence of the CW mass on the spectrum of natural frequencies – model M2

f_n (Hz)	f_1	f_2	f_3	f_4	f_5	f_6	f_7	f_8	f_9	f_{10}	f_{11}	f_{12}	f_{13}
$m_{CW,DES}$	0.721	0.893	1.010	1.577	1.897	2.586	2.954	3.039	3.255	3.730	4.946	5.291	6.055
$m_{CW,ACT}$	0.709	0.871	0.980	1.562	1.847	2.586	2.954	3.039	3.254	3.730	4.761	5.240	6.037

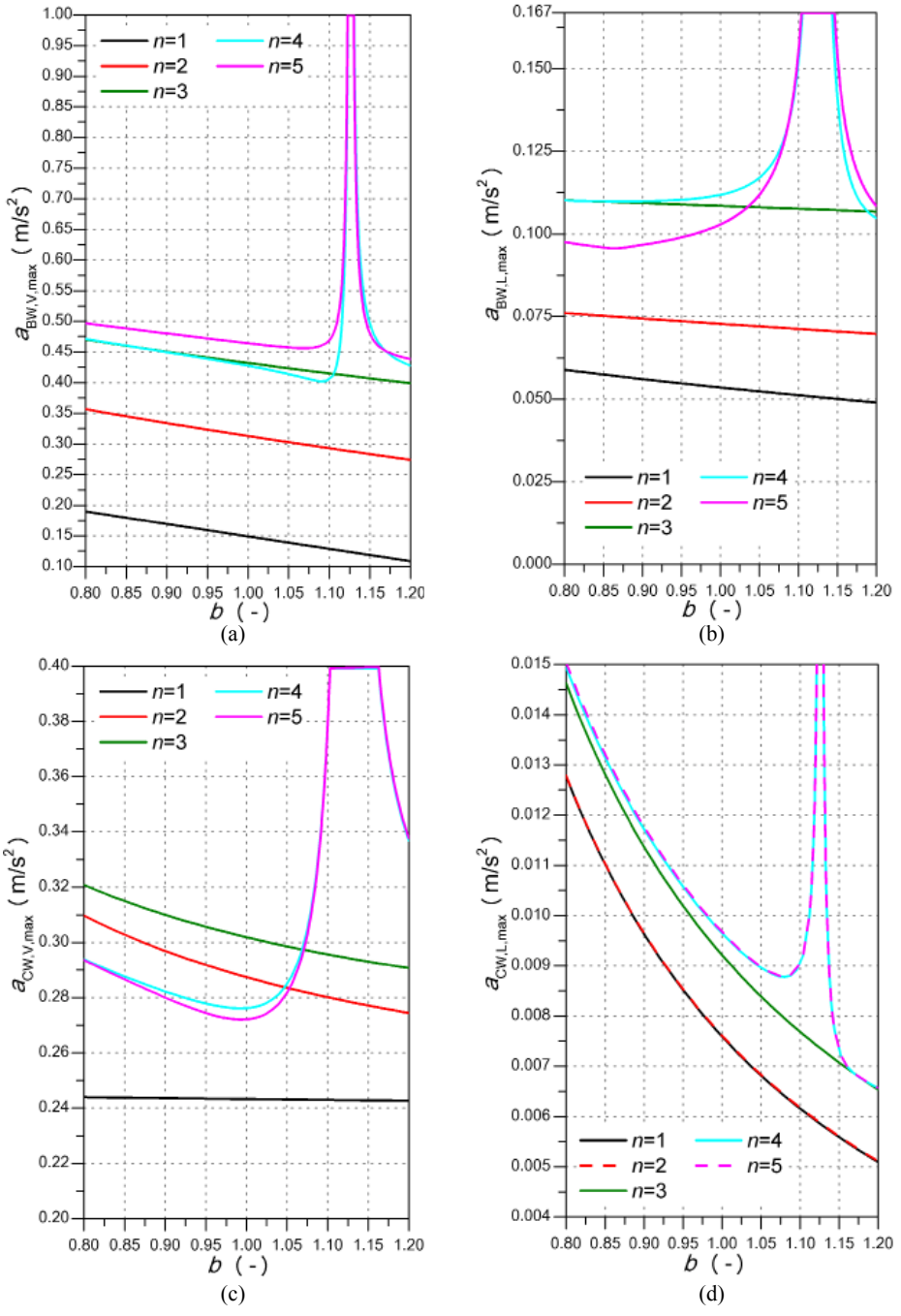

Fig. 7. Maximum values of vertical and lateral accelerations of referent points – model M1:
(a) vertical acceleration of the BWC; (b) lateral acceleration of the BWC;
(c) vertical acceleration of the CW COG; (d) lateral acceleration of the CW COG

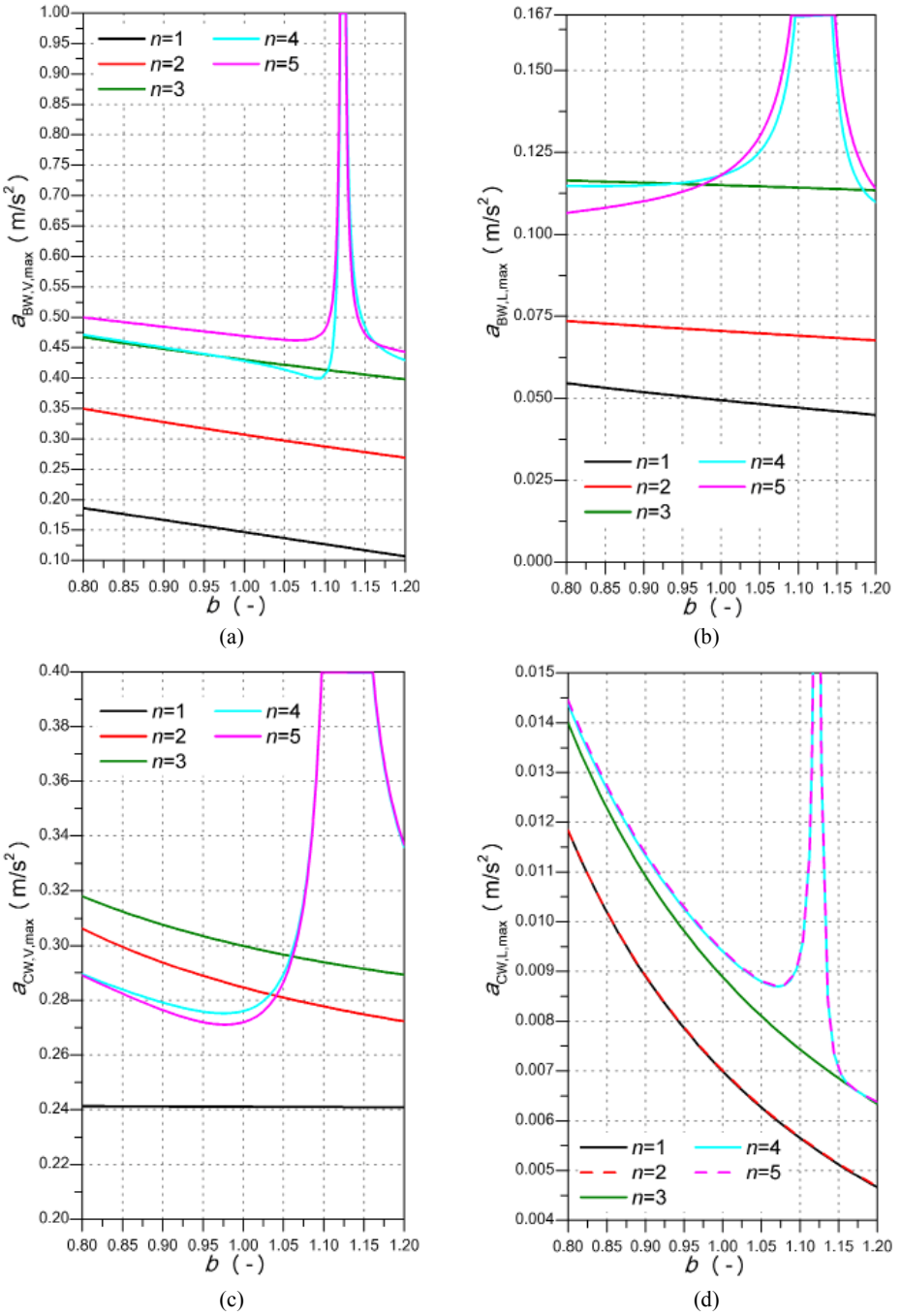

Fig. 8. Maximum values of vertical and lateral accelerations of referent points – model M2:
(a) vertical acceleration of the BWC; (b) lateral acceleration of the BWC;
(c) vertical acceleration of the CW COG; (d) lateral acceleration of the CW COG

TABLE 4

Maximum values of accelerations for $m_{CW,DES}$ (b_{DES} = 0.83) and $m_{CW,ACT}$ (b_{ACT} = 1) – model M1

n	$a_{BW,V,max}$ (m/s^2)		$a_{BW,L,max}$ (m/s^2)		$a_{CW,V,max}$ (m/s^2)		$a_{CW,L,max}$ (m/s^2)	
	$m_{CW,DES}$	$m_{CW,ACT}$	$m_{CW,DES}$	$m_{CW,ACT}$	$m_{CW,DES}$	$m_{CW,ACT}$	$m_{CW,DES}$	$m_{CW,ACT}$
1	0.184	0.149	0.058	0.054	0.244	0.243	0.012	0.008
2	0.350	0.313	0.076	0.073	0.306	0.287	0.012	0.008
3	0.464	0.432	0.110	0.109	0.317	0.302	0.014	0.009
4	0.465	0.427	0.110	0.112	0.290	0.276	0.014	0.010
5	0.492	0.464	0.097	0.103	0.290	0.272	0.014	0.010

TABLE 5

Maximum values of accelerations for $m_{CW,DES}$ (b_{DES} = 0.83) and $m_{CW,ACT}$ (b_{ACT} = 1) – model M2

n	$a_{BW,V,max}$ (m/s^2)		$a_{BW,L,max}$ (m/s^2)		$a_{CW,V,max}$ (m/s^2)		$a_{CW,L,max}$ (m/s^2)	
	$m_{CW,DES}$	$m_{CW,ACT}$	$m_{CW,DES}$	$m_{CW,ACT}$	$m_{CW,DES}$	$m_{CW,ACT}$	$m_{CW,DES}$	$m_{CW,ACT}$
1	0.181	0.147	0.054	0.049	0.241	0.241	0.011	0.007
2	0.343	0.307	0.073	0.071	0.302	0.285	0.011	0.007
3	0.462	0.430	0.116	0.115	0.315	0.300	0.013	0.009
4	0.465	0.428	0.115	0.118	0.286	0.276	0.013	0.009
5	0.495	0.469	0.107	0.118	0.285	0.272	0.013	0.009

4. Discussion

All of the analyzed natural frequencies, for both analyzed models, are monotonously decreasing with the increase of the CW mass, which was an expected result considering the overall increase of the models masses, Figs. 5 and 6, Tables 2 and 3. Eleventh natural frequency is the most sensitive to the variation of the CW mass for both analyzed models, Table 6, with percentage decrease of –3.9%. Third natural frequency is slightly more sensitive for M2 (–3.1%) compared to the M1 (–2.9%) model. Sensitivity of all the other natural frequencies is less than –3%. It is observed that sixth through tenth natural frequencies are practically insensitive to the variation of the CW mass.

TABLE 6

Percentage decrease of models' natural frequencies provoked by the increase of the CW mass

Model	Percentage difference	Natural frequency												
		n												
		1	2	3	4	5	6	7	8	9	10	11	12	13
M1	$\frac{f_n^{b_{ACT}} - f_n^{b_{DES}}}{f_n^{b_{DES}}} \times 100$	–1.8	–2.7	–2.9	–1.0	–2.6	0.0	0.0	0.0	0.0	0.0	–3.9	–0.8	–0.3
M2		–1.7	–2.5	–3.1	–1.0	–2.7	0.0	0.0	0.0	0.0	0.0	–3.9	–1.0	–0.3

The influence of transition from the designed image (DI) of the superstructure (model M1 with CW mass of $m_{CW,DES}$ = 197 t), Fig 5 and Table 2, to the actual image (AI) of the super-

structure (model M2 with CW mass of $m_{CW,ACT}$ = 238 t), Fig 6 and Table 3, on the free vibration frequencies is presented in Table 7. All of the analyzed natural frequencies are lower for the AI compared to the DI. The transition has the highest influence on the third, fifth and eleventh natural frequencies (–3.2%, –3.0% and –4.0%, respectively). From the engineering point of accuracy, sixth through tenth and the thirteenth natural frequencies are practically insensitive to the transition from DI to the AI of the superstructure.

TABLE 7

Designed (DI) vs. actual (AI) image of the superstructure – the influence on the spectrum of free vibration frequencies

Percentage difference	**Natural frequency**												
	n												
	1	**2**	**3**	**4**	**5**	**6**	**7**	**8**	**9**	**10**	**11**	**12**	**13**
$\frac{f_n^{AI} - f_n^{DI}}{f_n^{DI}} \times 100$	–2.2	–2.9	–3.2	–1.5	–3.0	–0.1	–0.1	0.0	–0.1	–1.0	–4.0	–1.9	–1.0

There are no resonances in the range of the analyzed parameter between b_{DES} and b_{ACT}, neither for the M1 nor the M2 model. However, should the CW mass be higher than the actual CW mass, by 12.6% for model M1, Fig. 5(b), and by 12.2% for model M2, Fig. 6(b), the fourth order resonant state would appear. Third natural frequency of both models is the closest to the first frequency of excitation, Figs. 5(a) and 6(a). The ratio of mentioned frequencies has the lowest value for b_{DES} and equals to ≈1.14, Table 8. The sixth natural frequency of both models is the closest to the frequency of the second excitation harmonic with the ratio of ≈0.89 ($b = b_{DES}$). Accordingly, it is conclusive that in the low frequency region (up to 3 Hz), Figs. 5(a) and 6(a), the construction is oscillating in the region unaffected by the first and second order resonances. Although the values of ratios ψ_3, ψ_4 and ψ_5, Table 8, are in close proximity to 1, the influence of the third, fourth and fifth excitation frequencies on the dynamic response of the superstructure is not significant, for $b \in [b_{DES}, b_{ACT}]$, Figs. 7 and 8.

TABLE 8

Ratios between the values of excitation frequencies and the closest values of natural frequencies

Model	**Ratio between frequency of excitation and the closest natural frequency**				
	$\psi_1 = f_{1,e}/f_3$ ($b = b_{DES}$)	$\psi_2 = f_{2,e}/f_6$ ($b = b_{DES}$)	$\psi_3 = f_{3,e}/f_9$ ($b = b_{DES}$)	$\psi_4 = f_{4,e}/f_{11}$ ($b = b_{ACT}$)	$\psi_5 = f_{5,e}/f_{13}$ ($b = b_{ACT}$)
M1	1.143	0.893	1.065	0.970	0.951
M2	1.146	0.894	1.066	0.972	0.958

In the same domain of parameter b variation, maximum values of accelerations of the referent points, Tables 4 and 5, are lower than the limiting (permitted) values prescribed by the standard (DIN 22261-2, 2016), Table 9. In addition, maximum values of lateral CW COG accelerations are considerably lower than the permitted acceleration and are not of interest for further analysis. Mass of the CW has an influence on the maximum intensities of the referent points' accelerations, Table 10. An increase of the CW mass, to which the sensitivity of the M1 model is slightly

higher, leads to the decrease of maximum values of vertical accelerations (up to –6.2% in case of $a_{CW,V,max}$). In contrast, the increase of the CW mass leads to the increase in maximum values of the BWC lateral accelerations, to which the sensitivity of the M2 model (10.3%) is significantly higher compared to the sensitivity of the M1 model (6.2%).

TABLE 9

Permitted (limiting) acceleration values according to the standard (DIN 22261-2, 2016)

Vertical direction: $a_{V,per}$ (m/s^2)		**Lateral direction: $a_{L,per}$ (m/s^2)**	
Model referent points			
BW	CW	BW	CW
1	0.4	0.167	0.333

TABLE 10

Percentage difference $100 \times (a_{m,CW,ACT} - a_{m,CW,DES})/a_{m,CW,DES}$ (%)

Model	$a_{BWC,V,max}$	$a_{BWC,L,max}$	$a_{CW,V,max}$
M1	–5.7	6.2	–6.2
M2	–5.3	10.3	–4.6

From the aspect of digging resistance approximation accuracy, Fig. 3, Table 1, it is conclusive that, already for $n = 2$, Fourier series yields the approximation of the maximum values with the absolute error value lower than 3%, which is acceptable from the engineering standpoint. However, when maximum values of the referent points' accelerations are analyzed, the level of the error is considerably higher. The following is conclusive on the basis of calculation results presented in Table 11: (a) the maximum level of error, obtained for the maximum acceleration values when $n = 2$, compared to $n = 5$, is by an order of magnitude higher (–39.8%) then the level of error made for the same number of members in the trigonometric polynomials used for the approximation of the digging resistance (–2.68%); (b) maximum accelerations of the BWC are much more sensitive (up to –39.8%) to the number of members of the approximation polynomial for the digging resistance than maximum vertical accelerations of the CW COG (up to 6.0%); (c) model M2 is more sensitive to the number of members of the digging resistance approximation polynomial, except in the case of maximum vertical accelerations of the CW COG for $m_{CW} = m_{CW,ACT}$.

TABLE 11

Percentage difference $100 \times (a_{n=2} - a_{n=5})/a_{n=5}$ (%)

Model	$a_{BWC,V,max}$		$a_{BWC,L,max}$		$a_{CW,V,max}$	
	$m_{CW,DES}$	$m_{CW,ACT}$	$m_{CW,DES}$	$m_{CW,ACT}$	$m_{CW,DES}$	$m_{CW,ACT}$
M1	–28.9	–32.5	–21.7	–29.1	5.5	5.5
M2	–30.1	–34.5	–31.8	–39.8	6.0	4.8

If maximum intensities of the DI accelerations are adopted as the basis for comparison, Table 12, it is observed that: (a) the number of members of digging resistance approximation

polynomial has a significant influence on the values of percentage deviations (in case of $a_{BWC,L,max}$ mentioned deviation is 3.3 times higher for $n = 5$ than for $n = 2$); (b) the maximum values of AI vertical accelerations are lower than corresponding values obtained for DI: for $n = 5$, maximum vertical accelerations of the BWC and CW COG are lower by 4.7% and 6.2%, respectively; (c) in contrast, maximum values of BWC lateral accelerations are 21.7% higher for the AI in case of $n = 5$. The decrease of maximum intensities of maximum vertical accelerations of the BWC and CW COG by 4.7% and 6.2%, respectively, emphasise that the AI of the superstructure is expressing a more favourable behaviour. Only the lateral acceleration of the BWC rises by 21.7% due to the transition of the structure. Having in mind the fact that the maximum intensities of vertical accelerations are closer to the permitted values, compared to the maximum values of maximum lateral accelerations and their respective limitations, Tables 4, 5 and 9, it is conclusive that the AI of the superstructure expresses a more favourable dynamic behaviour. Conclusion about a more favourable dynamic behaviour of the AI of the superstructure is valid only when the mass of the CW is equal to the actual. With the increase of the CW mass by more than 5.6%, the maximum vertical acceleration of the CW COG would exceed the value obtained for the DI of the superstructure, and the mentioned maximum acceleration would reach the permitted value for $b_{LIM} = 1.098$.

TABLE 12

Percentage difference $100 \times (a_{max,AI,n} - a_{max,DI,n})/a_{max,DI,n}$ (%)

n	$a_{BWC,V,max}$	$a_{BWC,L,max}$	$a_{CW,V,max}$
2	–12.2	6.6	–6.9
3	–7.3	4.5	–5.4
4	–7.9	7.3	–4.8
5	–4.7	21.7	–6.2

Maximum vertical accelerations of the BWC, for both of the analyzed models, Figs. 7(a) and 8(a) and Tables 4 and 5, are increasing with the increase in the number of members in the Fourier series, when $b = b_{DES}$. The influence of the fourth order resonance, indicated by the rise of the value of acceleration by only 0.2% and 0.6% for M1 and M2, respectively, when the system is subjected to the action of generalized non-potential forces developed up to the third member of Fourier series ($n = 3$) compared to the fourth ($n = 4$), is more obvious when the values of maximum vertical accelerations obtained for the end of the interval ($b = b_{ACT}$) are analyzed. The values are rising up to $n = 3$, Tables 4 and 5, and then, for $n = 4$, decreasing by 1.1% for M1 and 0.5% for M2. Similar trend is observed when analyzing maximum lateral accelerations of the BWC, Figs. 7(b) and 8(b) and Tables 4 and 5. The biggest decrease in the values of maximum accelerations is observed when comparing values obtained for $n = 4$ and $n = 5$ for both models at the beginning of the analyzed interval ($b = b_{DES}$), and is equal to 11.8% for M1 and 7.0% of M2. At the end of the analyzed interval ($b = b_{ACT}$), analyzed values are 8.0% lower for M1 and of equal value for M2. The decrease in maximum accelerations of both models with the increase of the number of members in the Fourier series is also observed when analyzing maximum vertical accelerations of the CW COG, Figs. 7(c) and 8(c) and Tables 4 and 5. At the beginning of the interval ($b = b_{DES}$), values obtained for M1 and M2 and $n = 5$ are 8.5% and 9.5% lower than those obtained for the $n = 3$. At the end of the interval ($b = b_{ACT}$) analyzed values are 9.9% and 9.3%

lower. At the adopted level of calculation accuracy, no conclusions can be made regarding the influence of the fourth order resonance on the maximum lateral accelerations of the CW COG, Figs. 7(d) and 8(d) and Tables 4 and 5.

5. Conclusion

Having in mind the facts that (a) the values of natural frequencies are of the same order of magnitude and (b) the corresponding deflection shapes are in full compliance in comparison with the experimentally-analyzed bucket wheel excavators of the same conceptual design, it is concluded that the developed reduced spatial dynamic models of the bucket wheel excavator with two masts describe the dynamic character of the superstructures with sufficient accuracy regardless of the higher values of natural frequencies of the analyzed models, which is explained by the differences in masses of the respective superstructures.

On basis of the comparative analysis of the results obtained by a numerical investigation of the designed (DI) and the actual (AI) model of the slewing superstructure with two masts, the following conclusions are made:

- the counterweight mass has an influence on the values of the analyzed spectrum of natural frequencies of up to 4%;
- the mass of the counterweight has a significant influence on the maximum intensities of maximum accelerations (up to 10.3%);
- no resonances have been observed in the domain of counterweight mass variation from the designed to the actual one, whereby maximum intensities of accelerations are lower than the limiting accelerations prescribed by the code DIN 22261-2;
- the maximum lateral acceleration intensities of the counterweight centre of gravity are considerably lower than the limiting acceleration value prescribed by the code DIN 22261-2;
- the appearance of a resonance is possible when the mass of the counterweight is increased by ≈12% of the actual value;
- for the 'a posteriori' model, the maximum vertical accelerations of the counterweight centre of gravity reach the limiting value prescribed by the code DIN 22261-2 for the counterweight mass 9.8% higher than the actual;
- Fourier series for $n = 2$ gives an approximation of maximum value of the digging resistance with an absolute error value lower than 3%, which is acceptable from the engineering standpoint;
- maximum level of error, obtained for the maximum intensities of maximum accelerations when $n = 2$, compared to $n = 5$, is by an order of magnitude higher (–39.8%) then the level of error which is made for the same number of members in the trigonometric polynomials used for the approximation of the digging resistance (–2.68%);
- judgement about the number of members in the Fourier series used to form the approximate trigonometric polynomial of the digging resistance, which describes the dynamic response of the superstructure accurately enough, cannot be made on the basis of accuracy of the excitation approximation, but on the basis of the system response analysis.

Acknowledgments

This work is a contribution to the Ministry of Education, Science and Technological Development of Serbia funded project TR 35006.

References

AS4324.1, 1995. *Mobile equipment for continuous handling of bulk materials Part 1 – General requirements for the design of steel structures*. Standards Australia.

Bošković S., Jovančić P., Ignjatović D., Rakićević B., Maneski T., 2015. *Vibration as deciding parameter during revitalization process for replacing the bucket wheel drive*. Journal of Vibroengineering **17**, 1, 24-32.

Bošnjak S., Oguamanam D., Zrnić N., 2006. *On the dynamic modelling of bucket wheel excavators*. FME Transactions **34**, 4, 221-226.

Bošnjak S., Zrnić N., 2012. *Dynamics, failures, redesigning and environmentally friendly technologies in surface mining systems.* Archives of Civil and Mechanical Engineering **12**, 3, 348-359.

Bošnjak S., 2015. *Comments on "Determination and analysis of the theoretical production of a bucket wheel excavator".* Archives of Mining Sciences **60**, 1, 283-301.

Bošnjak S.M., Oguamanam D.C.D., Zrnić N.Đ., 2015. *The influence of constructive parameters on response of bucket wheel excavator superstructure in the out-of-resonance region.* Archives of Civil and Mechanical Engineering **15**, 4, 977-985.

Bošnjak S., Gnjatović N., 2016. *The influence of geometric configuration on response of the bucket wheel excavator superstructure.* FME Transactions **44**, 3, 313-323.

Bošnjak S., Gnjatović N., Savićević S., Pantelić M., Milenović I., 2016. *Basic parameters of the static stability, loads and strength of the vital parts of the bucket wheel excavator's slewing superstructure.* Journal of Zhejiang University-SCIENCE A **17**, 5, 353-365.

Brkić A., Maneski T., Ignjatović D., Jovančić P., Spasojević Brkić V., 2014. *Diagnostics of bucket wheel excavator discharge boom dynamic performance and its reconstruction.* Eksploatacja i Niezawodność – Maintenance and Reliability **16**, 2, 188-197.

Che Z.X., Chen Y.L., 2014. *Determination and analysis of the theoretical production of a bucket wheel excavator*. Archives of Mining Sciences **59**, 1, 283-291.

Cireş I., Nani V.M., 2016. *Stability control for a huge excavator for surface excavation.* Applied Mathematical Modelling **40**, 1, 388-397.

DIN 22261-2, 2016. Excavators, Stackers and Auxiliary Equipment in Brown Coal Open Cut Mines Part 2 – Calculation Principals. German Institute for Standardization.

Dudek D., Frydman S., Huss W., Pękalski G., 2011. *The L35GSM cast steel – possibilities of structure and properties shaping at the example of crawler links.* Archives of Civil and Mechanical Engineering **11**, 1, 19-32.

Gnjatović N., 2016. *Influence of constructional parameters and parameters of excitation on response of the bucket wheel excavator with two masts in the out-of-resonance region*. Ph.D. dissertation. University of Belgrade – Faculty of mechanical engineering, Belgrade, Serbia.

Gottvald J., 2010. *The calculation and measurement of the natural frequencies of the bucket wheel excavator SchRs 1320/4x30.* Transport **25**, 3, 269-277.

Gottvald J., 2011. *Measuring and Comparison of Natural Frequencies of Bucket Wheel Excavators SchRs 1320 and K 2000.* GEMESED'11 – Proceedings of the 4th WSEAS international conference on Energy and development – environment – biomedicine, Corfu Island, Greece, 335-340.

Gottvald J. 2012. *Analysis of vibrations of bucket wheel excavator SchRs 1320 during mining process.* FME Transactions **40**, 4, 165-170.

Machniak Ł., Kozioł W., 2017. *Method of assessment of hard rock workability using bucket wheel excavators*, Archives of Mining Sciences **62**, 1, 73-82.

Pietrusiak D., 2013. *Analiza modalna w ocenie dynamiki ustroju wielonaczyniowych koparek kołowych*. Ph.D. dissertation., Politechnika Wrocławska, Wroclaw, Poland.

Pietrusiak D., Moczko P., Czmochowski J., 2014. *Field and Numerical Testing of the BWE SchRs4600.50 Dynamic Behavior*. In: Allemang R. et al. (eds.) Topics in Modal Analysis, Vol. 7, Springer, New York, 525-532.

Pietrusiak D., 2017. *Evaluation of large-scale load-carrying structures of machines with the application of the dynamic effects factor.* Eksploatacja i Niezawodność – Maintenance and Reliability **19**, 4, 542-551.

Rasper L., 1973. *Der Schaufelradbagger als Gewinnungsgerat*. Trans. Tech. Publications, Clausthal, Germany.

Rusiński E., Czmochowski J., Iluk A., Kowalczyk M., 2010. *An analysis of the causes of a BWE counterweight boom support fracture.* Engineering Failure Analysis **17**, 1, 179-191.

Rusiński E., Dragan S., Moczko P., Pietrusiak D., 2012. *Implementation of experimental method of determining modal characteristics of surface mining machinery in the modernization of the excavating unit.* Archives of Civil and Mechanical Engineering **12**, 4, 471-476.

Rusiński E., Czmochowski J., Moczko P., Kowalczyk M., Pietrusiak D., Przybyłek G., Smolnicki T., Stańco M., 2015. *Ocena stanu technicznego maszyn podstawowych górnictwa odkrywkowego*. Oficyna wydawnicza politechniki wrocławskiej, Wroclaw, Poland.

Rusiński E, Czmochowski J, Moczko P, Pietrusiak D., 2017. *Surface Mining Machines – Problems of Maintenance and Modernization*. Springer International Publishing AG, Cham, Switzerland.

Savković M., Gašić M., Arsić M., Petrović R., 2011. *Analysis of the axle fracture of the bucket wheel excavator.* Engineering Failure Analysis **18**, 1, 433-441.

Schlecht B., 2014. *Untersuchung und Optimierung des dynamischen Verhaltens von Schaufelradantrieben*. Final report of the research project 16575 BR funded by the Federal Ministry for Economics Affairs and Energy of Germany.

Volkov D.P., Cherkasov, V.A., 1969. *Динамика и прочность многоковшовых экскаваторов и отвалообразователей*. Машиностоение, Moscow, Russia.